Sparse PEC Scatterers Retrieval by means of a Local Shape Function Bayesian Compressive Sensing Strategy

L. Poli, G. Oliveri, A. Massa

Abstract

This report proposes an analysis on the dependence of the performances of the the local shape function multi-task Bayesian compressive sensing method on the number of scattering data when various measurement setups different from the optimal one have been considered, in order to show the effectiveness of the compressive sensing-based methodology when dealing with few data. Comparison with the single-task Bayesian compressive sensing implementation are also proposed.

1 Varying the Number of Views

Goal: show the performances of BCS when dealing with a sparse scatterer

- Number of Views: V
- Number of Measurements: M
- Number of Cells for the Inversion: N
- Number of Cells for the Direct solver: D
- Side of the investigation domain: L

Test Case Description

Direct solver:

- Square domain divided in $\sqrt{D} \times \sqrt{D}$ cells
- Domain side: $L = 3\lambda$
- $D = 1296$ (discretization for the direct solver: $< \lambda/10$)

Investigation domain:

- Square domain divided in $\sqrt{N} \times \sqrt{N}$ cells
- $L = 3\lambda$
- $2ka = 2 \times \frac{2\pi}{\lambda} \times \frac{L\sqrt{2}}{2} = 26.66$
- $\#DOF = \frac{(2ka)^2}{2} = \frac{(2\times\frac{2\pi}{\lambda}\times\frac{L\sqrt{2}}{2})^2}{2} \approx 364.5$
- N scelto in modo da essere vicino a $\#DOF$: $N = 324$ (18×18)

Measurement domain:

- Measurement points taken on a circle of radius $\rho = 3\lambda$
- Full-aspect measurements
- $M \approx 2ka \rightarrow M = 27$

Sources:

- Plane waves
- $V \in \{2, 3, 4, 5, 6, 7, 8, 9, 10, 11, 12, 13, 14, 15, 16, 17, 18, 19, 20, 21, 22, 23, 24, 25, 26, 27\}$
- Amplitude: $A = 1$
- Frequency: 300 MHz ($\lambda = 1$)

PEC Objects:

- $S = 1, 4, 8$ Sparse square cylinders of side $\frac{\lambda}{6} \cong 0.16\lambda$

MT-BCS-based technique parameters:

- Gamma prior on noise variance parameter: $a = 5 \times 10^{-2}$
- Gamma prior on noise variance parameter: $b = 5 \times 10^{-2}$
- Convergenze parameter: $\tau = 1.0 \times 10^{-8}$
- Threshold: $\eta = 0.27$

Varying the Number of Views, $S = 1$ - Error Figures

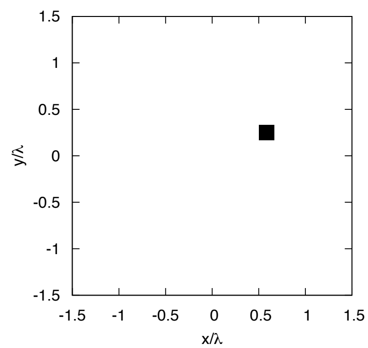

Figure 26. Actual object

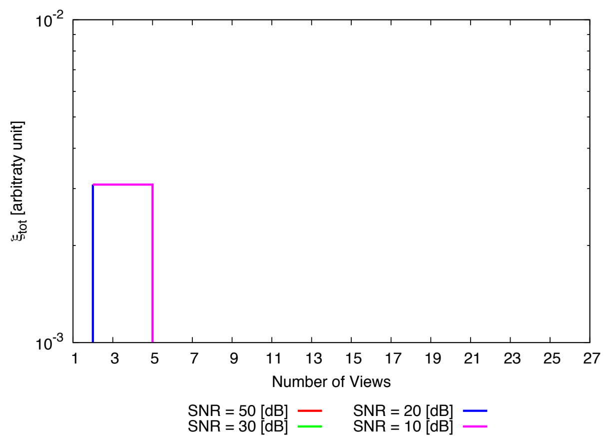

(a)

(Empty Figure)

(b)

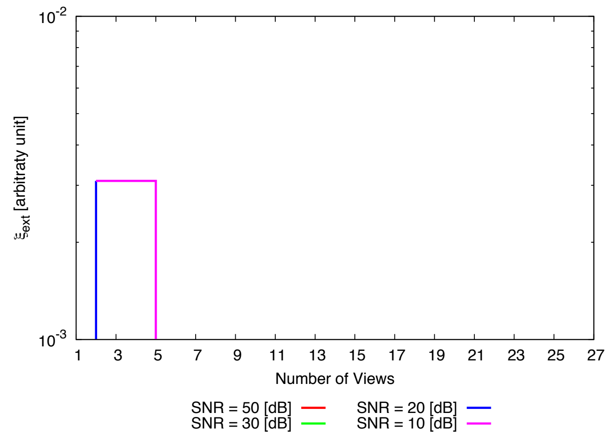

(c)

Figure 1. Behavior of the total error ξ_{tot} (a), internal error ξ_{int} (b) and external error ξ_{ext} (c) as a function of V.

Varying the Number of Views, $S = 4$ - Error Figures

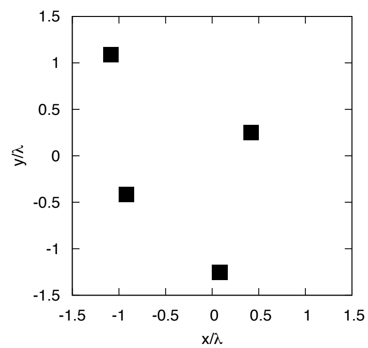

Figure 28. Actual object

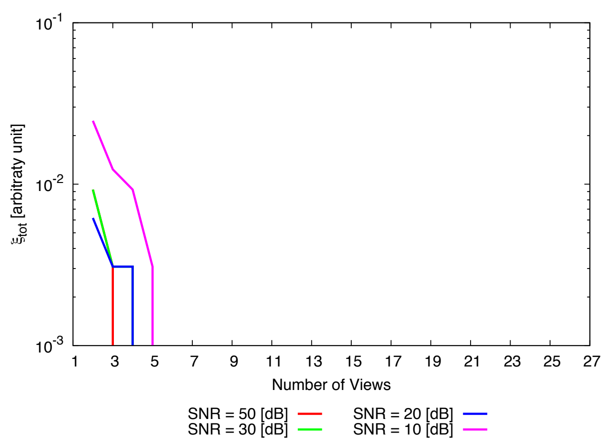

(*a*)
(Empty Figure)

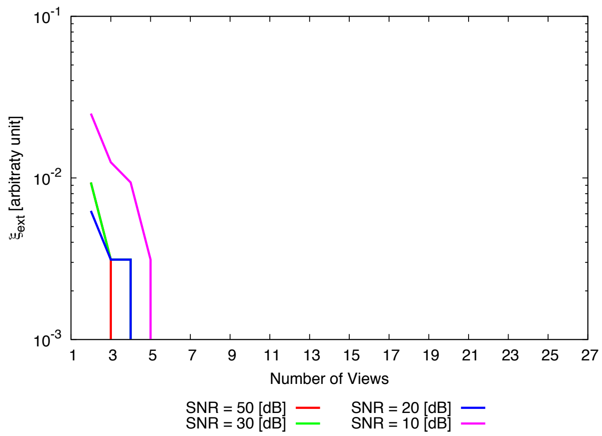

(c)

Figure 2. Behavior of the total error ξ_{tot} (a), internal error ξ_{int} (b) and external error ξ_{ext} (c) as a function of V.

1.1 Varying the Number of Views/Measurement Points

Goal: show the performances of BCS when dealing with a sparse scatterer

- Number of Views: V
- Number of Measurements: M
- Number of Cells for the Inversion: N
- Number of Cells for the Direct solver: D
- Side of the investigation domain: L

Test Case Description

Direct solver:

- Square domain divided in $\sqrt{D} \times \sqrt{D}$ cells
- Domain side: $L = 3\lambda$
- $D = 1296$ (discretization for the direct solver: $< \lambda/10$)

Investigation domain:

- Square domain divided in $\sqrt{N} \times \sqrt{N}$ cells
- $L = 3\lambda$
- $2ka = 2 \times \frac{2\pi}{\lambda} \times \frac{L\sqrt{2}}{2} = 26.66$
- $\#DOF = \frac{(2ka)^2}{2} = \frac{(2\times\frac{2\pi}{\lambda}\times\frac{L\sqrt{2}}{2})^2}{2} \approx 364.5$
- N scelto in modo da essere vicino a $\#DOF$: $N = 324$ (18×18)

Measurement domain:

- Measurement points taken on a circle of radius $\rho = 3\lambda$
- Full-aspect measurements
- $M \in \{2, 3, 4, 5, 6, 7, 8, 9, 10, 11, 12, 13, 14, 15, 16, 17, 18, 19, 20, 21, 22, 23, 24, 25, 26, 27\}$

Sources:

- Plane waves
- $V = M$
- Amplitude: $A = 1$
- Frequency: 300 MHz ($\lambda = 1$)

PEC Objects:

- $S = 1, 4, 8$ Sparse square cylinders of side $\frac{\lambda}{6} \cong 0.16\lambda$

MT-BCS-based technique parameters:

- Gamma prior on noise variance parameter: $a = 5 \times 10^{-2}$
- Gamma prior on noise variance parameter: $b = 5 \times 10^{-2}$
- Convergenze parameter: $\tau = 1.0 \times 10^{-8}$
- Threshold: $\eta = 0.27$

Varying the Number of Views/Measurement Points, $S = 1$ - Error Figures

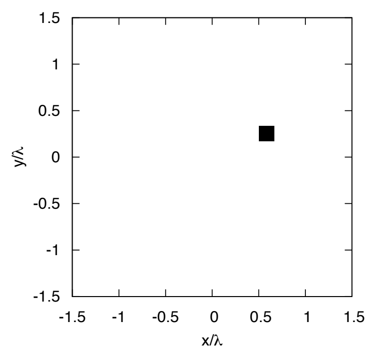

Figure 32. Actual object

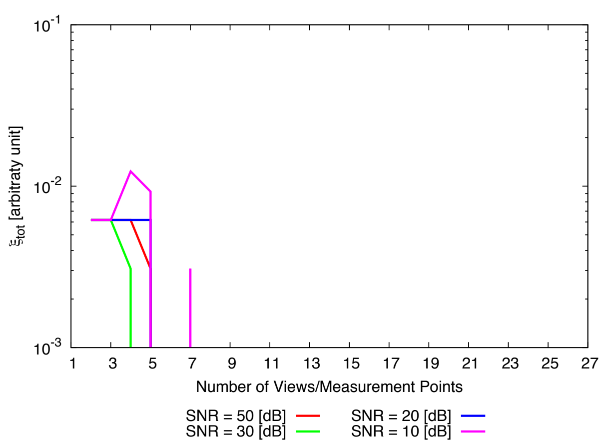

(a)

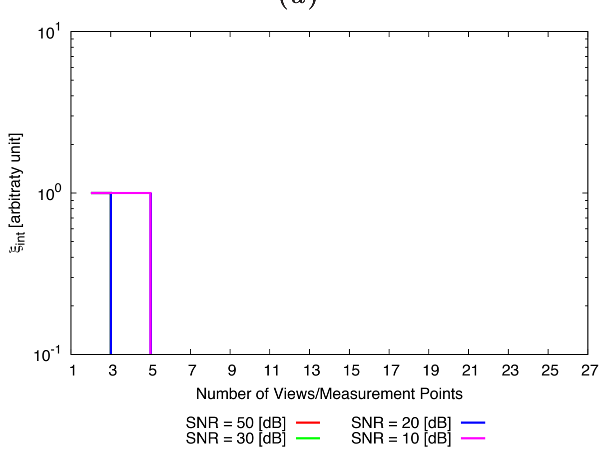

(b)

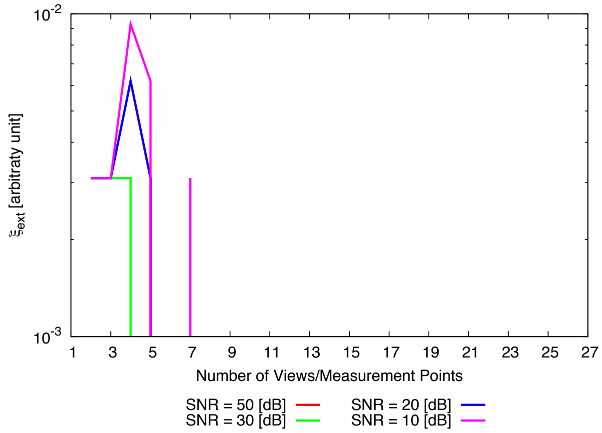

(c)

Figure 3. Behavior of the total error ξ_{tot} (a), internal error ξ_{int} (b) and external error ξ_{ext} (c) as a function of V.

Varying the Number of Views/Measurement Points, $S = 4$ - Error Figures

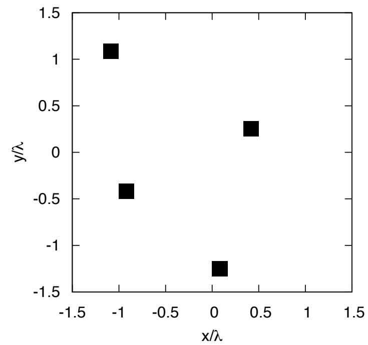

Figure 34. Actual object

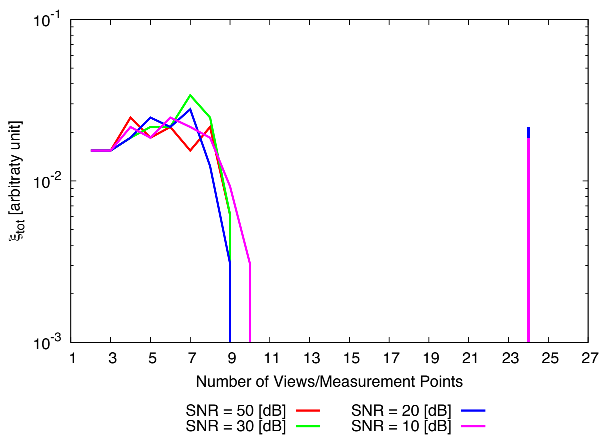

(a)

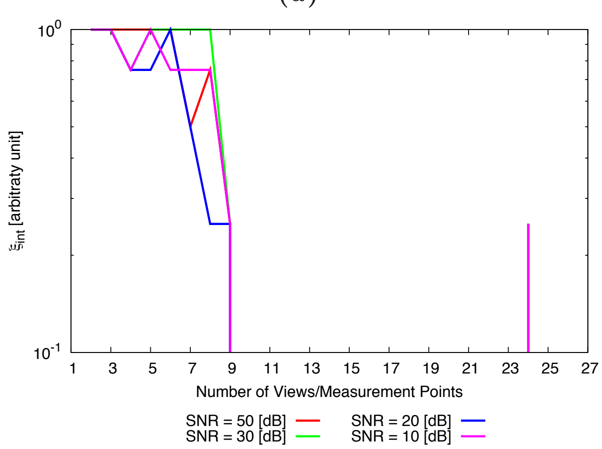

(b)

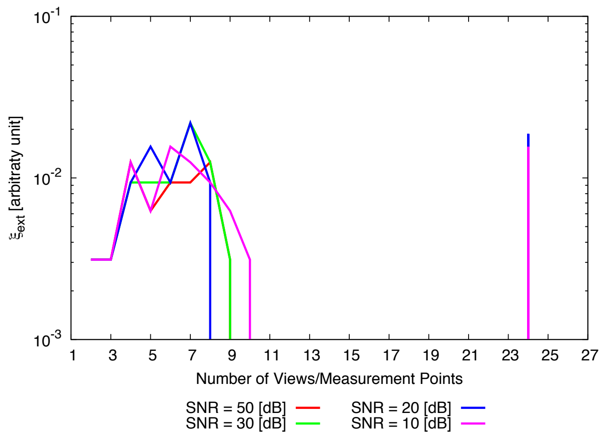

(c)

Figure 4. Behavior of the total error ξ_{tot} (a), internal error ξ_{int} (b) and external error ξ_{ext} (c) as a function of V.

2 Comparison with ST-BCS

2.1 L-shaped Cylinders

Goal: show the performances of BCS when dealing with a sparse scatterer

- Number of Views: V
- Number of Measurements: M
- Number of Cells for the Inversion: N
- Number of Cells for the Direct solver: D
- Side of the investigation domain: L

Test Case Description

Direct solver:

- Square domain divided in $\sqrt{D} \times \sqrt{D}$ cells
- Domain side: $L = 3\lambda$
- $D = 1296$ (discretization for the direct solver: $< \lambda/10$)

Investigation domain:

- Square domain divided in $\sqrt{N} \times \sqrt{N}$ cells
- $L = 3\lambda$
- $2ka = 2 \times \frac{2\pi}{\lambda} \times \frac{L\sqrt{2}}{2} = 6\pi\sqrt{2} = 26.65$
- $\#DOF = \frac{(2ka)^2}{2} = \frac{(2\times\frac{2\pi}{\lambda}\times\frac{L\sqrt{2}}{2})^2}{2} = 4\pi^2\left(\frac{L}{\lambda}\right)^2 = 4\pi^2 \times 9 \approx 355.3$
- N scelto in modo da essere vicino a $\#DOF$: $N = 324$ (18×18)

Measurement domain:

- Measurement points taken on a circle of radius $\rho = 3\lambda$
- Full-aspect measurements
- $M \approx 2ka \rightarrow M = 27$

Sources:

- Plane waves
- $V \approx 2ka \rightarrow V = 27$
- Amplitude: $A = 1$
- Frequency: 300 MHz ($\lambda = 1$)

PEC Object:

- L-shaped cylinder, 2 L-shaped cylinder

ST-BCS-based technique parameters:

- noise variance parameter: $\sigma^2 = 5 \times 10^{-3}$
- Convergenze parameter: $\tau = 1.0 \times 10^{-8}$
- Threshold: $\eta = 0.00$

Comparison ST-BCS/MT-BCS: 1 L-shaped Cylinder

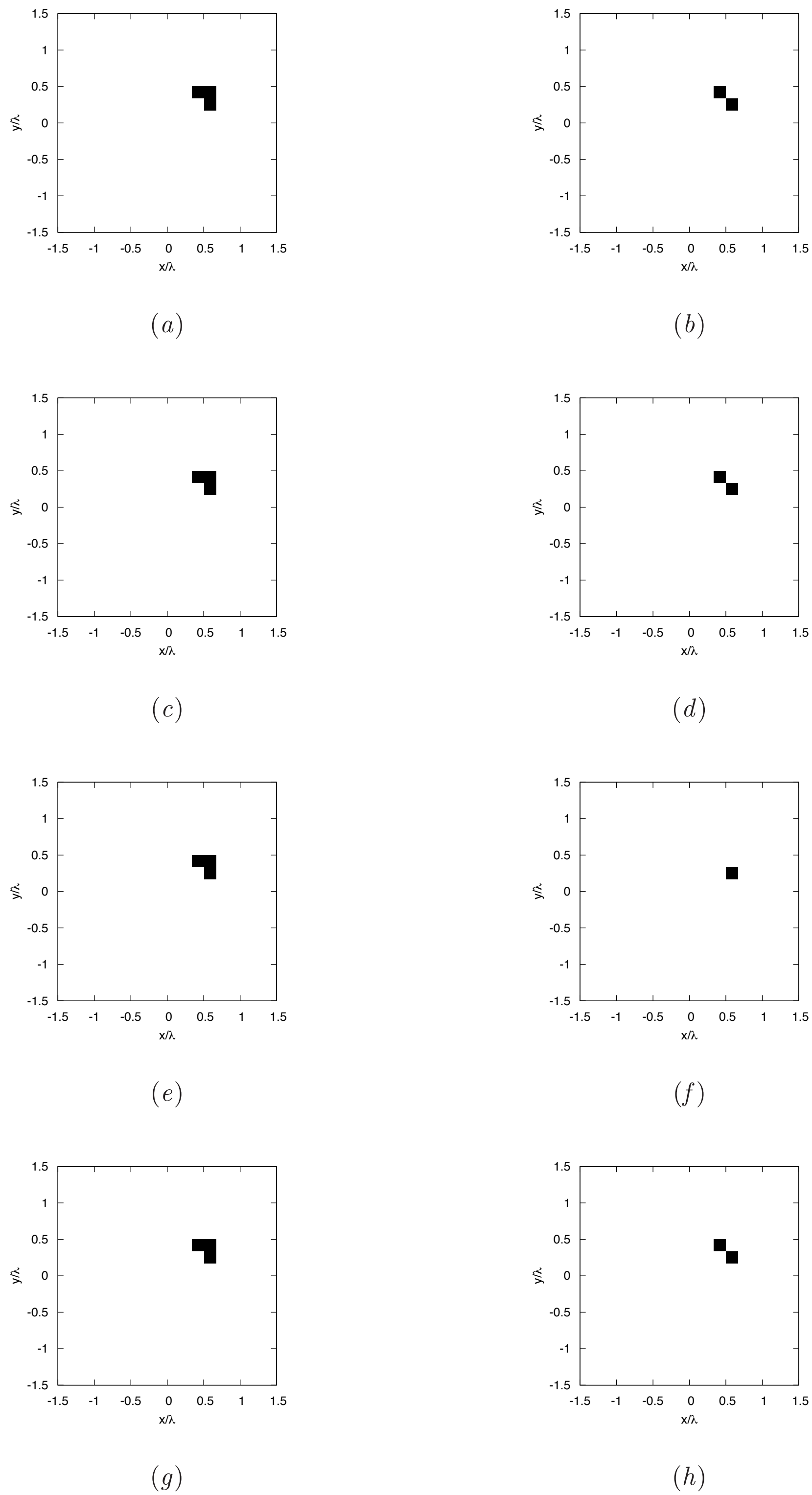

Figure 5. MT-BCS reconstructed object $(a)(c)(e)(g)$ and ST-BCS reconstructed object $(b)(d)(f)(h)$ for $SNR = 50$ [dB] $(a)(b)$, $SNR = 30$ [dB] $(c)(d)$, $SNR = 20$ [dB] $(e)(f)$ and $SNR = 10$ [dB] $(g)(h)$.

Comparison ST-BCS/MT-BCS: 2 L-shaped Cylinder

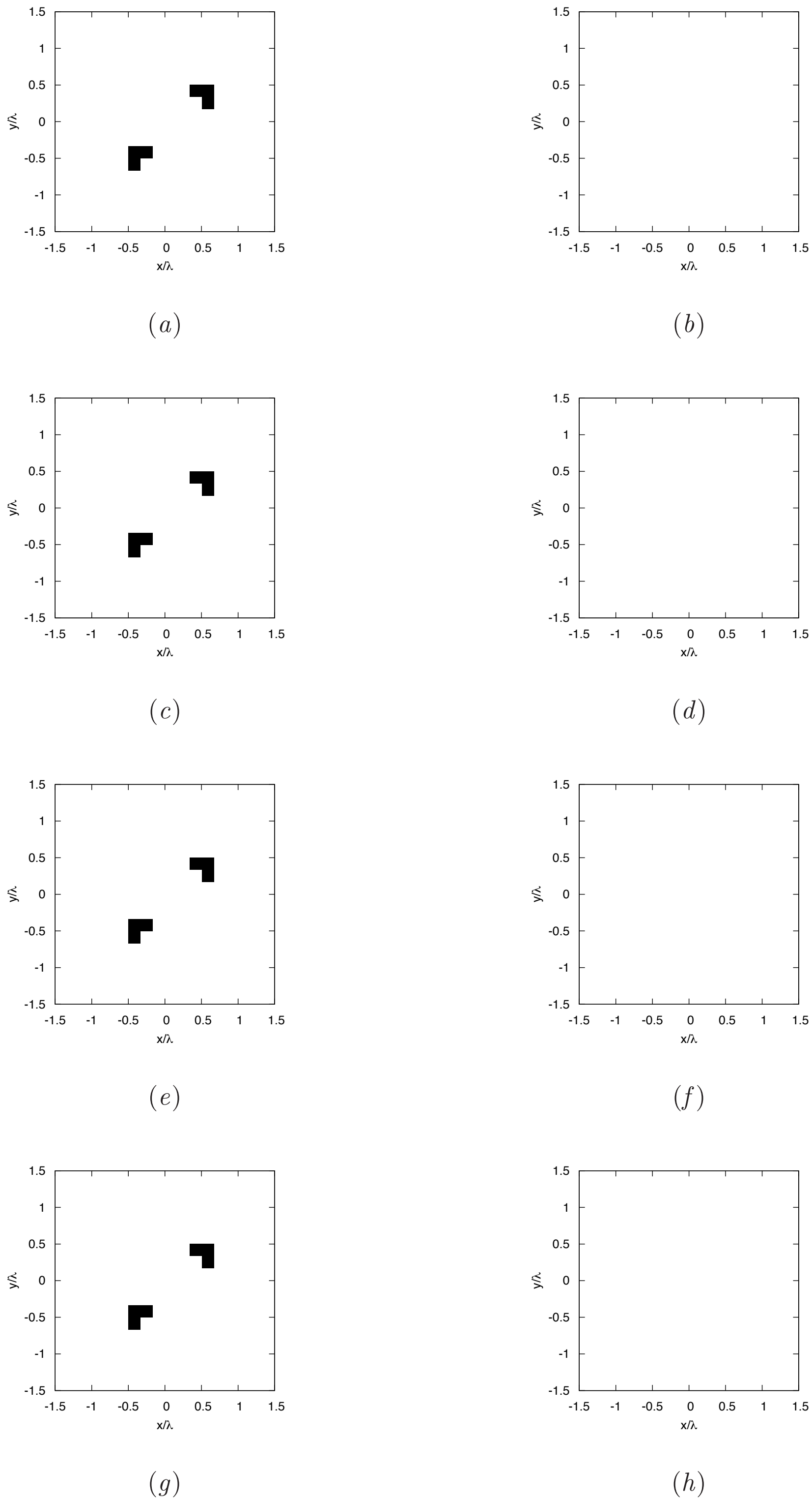

Figure 6. MT-BCS reconstructed object $(a)(c)(e)(g)$ and ST-BCS reconstructed object $(b)(d)(f)(h)$ for $SNR = 50$ [dB] $(a)(b)$, $SNR = 30$ [dB] $(c)(d)$, $SNR = 20$ [dB] $(e)(f)$ and $SNR = 10$ [dB] $(g)(h)$.

Observation:

- The reconstructions obtained using ST-BCS for the cases with 3 L-shaped and 4 L-shaped cylinders are the same as the ones obtained for the case with 2 L-shaped cylinders (Fig. 78 (b), (d), (f) and (h) - empty domain).

$1\,L-shaped\,Cylinders$					
	$SNR=50\,dB$	$SNR=40\,dB$	$SNR=30\,dB$	$SNR=20\,dB$	$SNR=10\,dB$
ξ_{tot}	3.09×10^{-3}	3.09×10^{-3}	3.09×10^{-3}	6.17×10^{-3}	3.09×10^{-3}
ξ_{int}	3.33×10^{-1}	3.33×10^{-1}	3.33×10^{-1}	6.66×10^{-1}	3.33×10^{-1}
ξ_{ext}	0.0	0.0	0.0	0.0	0.0

$2\,L-shaped\,Cylinders$					
	$SNR=50\,dB$	$SNR=40\,dB$	$SNR=30\,dB$	$SNR=20\,dB$	$SNR=10\,dB$
ξ_{tot}	1.85×10^{-2}	1.85×10^{-2}	1.85×10^{-2}	1.85×10^{-2}	1.85×10^{-2}
ξ_{int}	1.0	1.0	1.0	1.0	1.0
ξ_{ext}	0.0	0.0	0.0	0.0	0.0

$3\,L-shaped\,Cylinders$					
	$SNR=50\,dB$	$SNR=40\,dB$	$SNR=30\,dB$	$SNR=20\,dB$	$SNR=10\,dB$
ξ_{tot}	2.78×10^{-2}	2.78×10^{-2}	2.78×10^{-2}	2.78×10^{-2}	2.78×10^{-2}
ξ_{int}	1.0	1.0	1.0	1.0	1.0
ξ_{ext}	0.0	0.0	0.0	0.0	0.0

$4\,L-shaped\,Cylinders$					
	$SNR=50\,dB$	$SNR=40\,dB$	$SNR=30\,dB$	$SNR=20\,dB$	$SNR=10\,dB$
ξ_{tot}	3.70×10^{-2}	3.70×10^{-2}	3.70×10^{-2}	3.70×10^{-2}	3.70×10^{-2}
ξ_{int}	1.0	1.0	1.0	1.0	1.0
ξ_{ext}	0.0	0.0	0.0	0.0	0.0

Tab. II - ST-BCS Errors Resume: ξ_{tot}, ξ_{int} and ξ_{ext} for different values of SNR [dB].

References

[1] L. Poli, G. Oliveri, and A. Massa, "Imaging sparse metallic cylinders through a Local Shape Function Bayesian Compressive Sensing approach," Journal of Optical Society of America A, vol. 30, no. 6, pp. 1261-1272, 2013.

[2] F. Viani, L. Poli, G. Oliveri, F. Robol, and A. Massa, "Sparse scatterers imaging through approximated multitask compressive sensing strategies," Microwave Opt. Technol. Lett., vol. 55, no. 7, pp. 1553-1558, Jul. 2013.

[3] L. Poli, G. Oliveri, P. Rocca, and A. Massa, "Bayesian compressive sensing approaches for the reconstruction of two-dimensional sparse scatterers under TE illumination," IEEE Trans. Geosci. Remote Sensing, vol. 51, no. 5, pp. 2920-2936, May. 2013.

[4] L. Poli, G. Oliveri, and A. Massa, "Microwave imaging within the first-order Born approximation by means of the contrast-field Bayesian compressive sensing," IEEE Trans. Antennas Propag., vol. 60, no. 6, pp. 2865-2879, Jun. 2012.

[5] G. Oliveri, P. Rocca, and A. Massa, "A bayesian compressive sampling-based inversion for imaging sparse scatterers," IEEE Trans. Geosci. Remote Sensing, vol. 49, no. 10, pp. 3993-4006, Oct. 2011.

[6] G. Oliveri, L. Poli, P. Rocca, and A. Massa, "Bayesian compressive optical imaging within the Rytov approximation," Optics Letters, vol. 37, no. 10, pp. 1760-1762, 2012.

[7] L. Poli, G. Oliveri, F. Viani, and A. Massa, "MT-BCS-based microwave imaging approach through minimum-norm current expansion," IEEE Trans. Antennas Propag., vol. 61, no. 9, pp. 4722-4732, Sept. 2013.

[8] G. Oliveri, N. Anselmi, and A. Massa, "Compressive sensing imaging of non-sparse 2D scatterers by a total-variation approach within the Born approximation," IEEE Trans. Antennas Propag., 2014, submitted.

[9] S. C. Hagness, E. C. Fear, and A. Massa, "Guest Editorial: Special Cluster on Microwave Medical Imaging," IEEE Antennas Wireless Propag. Lett., vol. 11, pp. 1592-1597, 2012.

[10] A. Randazzo, G. Oliveri, A. Massa, and M. Pastorino, "Electromagnetic inversion with the multiscaling inexact-Newton method - Experimental validation," Microwave Opt. Technol. Lett., vol. 53, no. 12, pp. 2834-2838, Dec. 2011.

[11] M. Salucci, D. Sartori, N. Anselmi, A. Randazzo, G. Oliveri, and A. Massa, "Imaging buried objects within the second-order Born approximation through a multiresolution-regularized inexact-Newton method", in 2013 International Symposium on Electromagnetic Theory (EMTS), Hiroshima, Japan, pp. 116-118, May 20-24, 2013.